(2) the phase of the ESE signal for spin-correlated pairs differs from what is expected for spin pairs in thermodynamic equilibrium. The ESE phase of correlated pairs depends on the nature (degree) of spin excitation by the echo-forming RF pulses. For example, in the complete excitation case the shift in the ESE phase of spin-correlated pairs is close to $\pi/2$ relative to that of equilibrium spin pairs.

As mentioned earlier, at primary photosynthesis stages, not a single pair but a succession of electron-hole pairs forms. For this reason, time-resolved EPR spectra of two successive pairs have been calculated (model D). Some of the results are given in Figs 3 and 4 [11]. As in the single-pair situation, two successive pairs exhibit quantum beats in their EPR lines intensities. However, the intensity of the second pair has a different time dependence than it would be in the absence of the first pair. It is shown that the quantum beats for the second pair exhibit a phase shift. This shift appears even when, due to the relatively short lifetime of the first pair, its EPR spectrum is impossible to detect. Therefore the phase shift in EPR intensity oscillations of the radical pair may serve as a criterion for the existence of the preceding pair and enables the resonance parameters of this pair to be estimated.

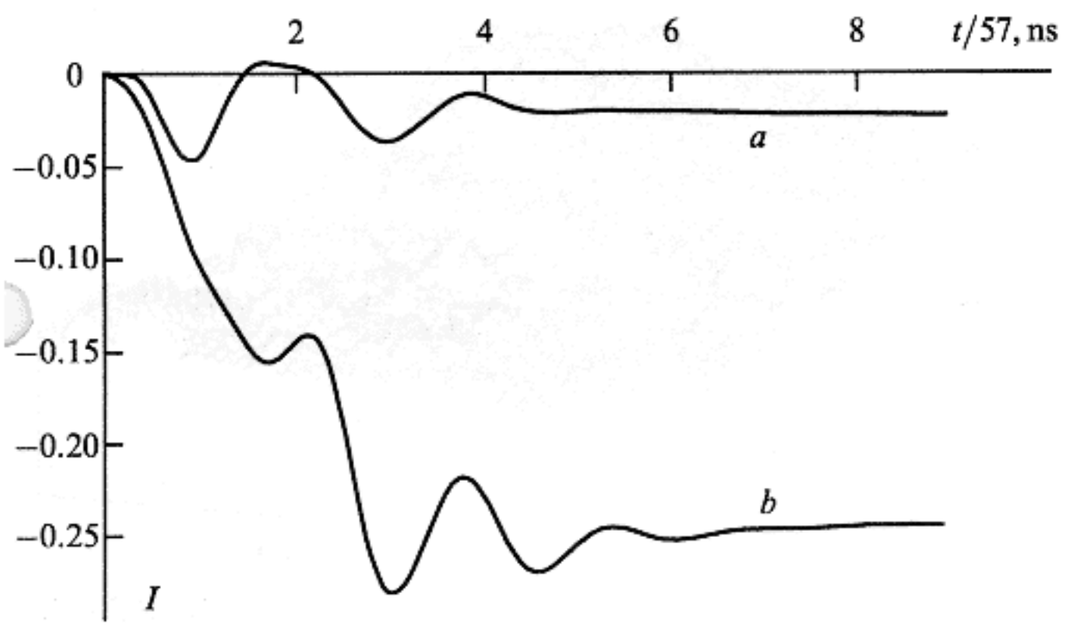

Figure 3. Time-resolved EPR spectrum for two independent radical pairs (*a*) and two successive pairs (*b*). In both cases the first pair forms right after the laser pulse and has an average lifetime $\tau_0 = 57$ ns, whereas the second pair emerges with a chemical reaction rate constant $k = 1/\tau_0$. The spectra are seen to differ greatly. There is a noticeable phase shift of EPR intensity beats for the successive pair compared to the spectrum of an independently created pair. Calculation parameters are typical for the EPR spectrometer X-range: for the first pair, $\omega_A/\gamma = 3003$ G, $\omega_B/\gamma = 3005$ G, $J/\gamma = 1$ G, $d = 0$; for the second pair, $\omega_A/\gamma = 3002$ G, $\omega_B/\gamma = 3006$ G, $J/\gamma = 0.1$ G, $d = 0$.

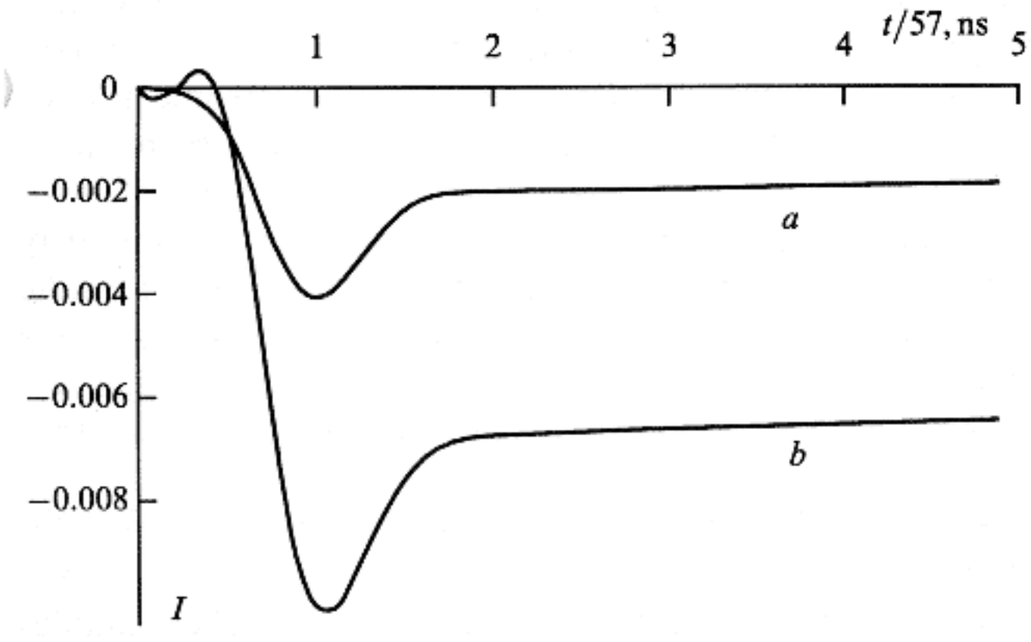

Figure 4. Time-resolved EPR spectrum for two independent radical pairs (*a*) and two successive pairs (*b*). In both cases the first pair forms right after the laser pulse and has an average lifetime of $\tau_0 = 57$ ns, whereas the second pair emerges with a chemical reaction rate constant $k = 1/\tau_0$. Unlike Fig. 3, the chemical reaction rate constant is an order of magnitude larger, so only the spectra from the second pairs are actually seen. Nevertheless, the phase of EPR intensity beats is shifted noticeably relative to the spectrum of an independently created pair. Calculation parameters are typical for the EPR spectrometer X-range: for the first pair, $\omega_A/\gamma = 3003$ G, $\omega_B/\gamma = 3005$ G, $J/\gamma = 1$ G, $d = 0$; for the second pair, $\omega_A/\gamma = 3002$ G, $\omega_B/\gamma = 3006$ G, $J/\gamma = 0.1$ G, $d = 0$.

References

1. *Advanced EPR. Applications in Biology and Biochemistry* (Ed. A J Hoff) (Amsterdam: Elsevier, 1989)
2. Fuchsle G et al. *Biochimica et Biophysica Acta* **1142** 23 (1993)
3. Norris J R, Schiffer M *Chemical and Engineering News* **68** (31) 22 (1990)
4. Salikhov K M *Usp. Fiz. Nauk* **160** (4)77 (1990) [*Sov. Phys. Usp.* **33** (4) 299 (1990)]
5. Salikhov K M, Bock C H, Shtelik D *Applied Magnetic Resonance* **1** 195 (1990)
6. Salikhov K M, Kandrashkin Yu E, Salikhov A K *Applied Magnetic Resonance* **3** 199 (1992)
7. Bittl R, Schulten K *Chem. Phys. Lett.* **173** (4) 387 (1991)
8. Bittl R et al. *Chem. Phys. Lett.* **226** 349 (1994)
9. Kothe G et al. in *Spin Chemistry* (Ed. Y J I'Haya) (Tokyo, 1991) pp. 420 – 434
10. Jeener J, Broekaert P *Phys. Rev.* **157** (2) 232 (1967)
11. 11. Kandrashkin Yu E, Salikhov K M, Shtelik D (to be published)

PACS numbers: 07.79.Cz, 07.79.Lh, 42.62.Hk

Scanning tunnelling and atomic force microscopy of surfaces modified by ion and laser beams

A A Bukharaev

1. Introduction

Scanning tunnelling and atomic force microscopes (STMs and AFMs) are finding increasing use in surface studies. This is explained by a number of unique advantages they offer, including a three-dimensional image of the surface; high (up to atomic scale) spatial resolution, not only in a superhigh vacuum but also in air; the possibility of studies both in a vacuum and in a liquid or gaseous medium, and, finally, working in the scanning tunnelling spectroscopy (STS) regime, which enables data on the distribution of electronic characteristics at the surface of a solid to be obtained.

STMs allow the investigations of the surface of a conducting medium. However, STM results obtained in the atmosphere should be regarded with some caution because of the strong effect of the adsorbed layers covering the surface in the air [1, 2]. Unlike STMs, AFMs provide high-resolution three-dimensional images of both conducting and nonconducting surfaces, but the surface distribution of electronic characteristics cannot as yet be studied with the same resolution as given by STMs.

This report presents the results obtained by the tunnelling microscopy group of the Kazan' Institute of Physics and Technology of RAS in STM and AFM studies on laser-modified Si and quartz-glass surfaces previously treated by ion etching.

In these studies, much attention has been given to the specifics of STM studies in air, notably to the effect of

adsorbed layers, whether natural or induced by the electric field of the STM needle, on STM/STS results. Besides, part of the work is concerned with the appearance (and methods for the elimination) of surface image distortions arising from the finite sizes of the STM and AFM needles.

The primary research objectives were to assess the reliability of STM-AFM data; to develop methods for reducing or eliminating possible image distortions; and to investigate processes at the implanted surface subject to a powerful laser pulse, from the viewpoint of using a given material in high-bit-density optical information record and storage.

The objects for the study were not chosen in a fortuitous manner. It is known that in certain ion implantation regimes the surface layer of Si becomes amorphous, the result being that the optical absorption coefficient of Si in the 1-μm range increases from 10^2 to 10^4 cm^{-1}. A similar effect was observed by us earlier [3] for the implantation of optical glasses by metal ions. The optical absorption coefficient of colourless optical glass in the visible and UV regions increased to 10^5 cm^{-1} after ion bombardment. In that case, the increase in the absorption coefficient is due to the formation of 5–100-nm metal particles in the implanted layer [3].

When such a medium is subject to a laser pulse, most of the energy is released in a thin high-absorptive implanted layer, thus producing a radiation sensitive material of good promise for optical information recording [4].

2. Experimental features of STM and AFM surface studies

Our investigations [1, 2] show that a major condition of the reliability of STM or STS data on the microtopography and electronic properties of Si requires that there be a tunnel contact between the STM needle and the Si surface. For an STM in air, such a contact may be produced by a special multistage passivation involving (i) the removal of the oxide layer and surface-contaminating hydrocarbons, and (ii) the hydrogen saturation of the active chemical bondings of the surface Si atoms [1]. Although a hydrogenated Si surface does not oxidise for several hours in air, the electric field of the STM needle may depassivate it as well as cause an intense deposition of adsorbates from the air onto the Si surface and the STM needle. This deteriorates considerably the quality of the STM image, as a consequence of the change in electron transport mechanism (Fig. 1). Our special studies [1, 2] indicated overbarrier Schottky emission as one of the mechanisms capable of satisfactorily explaining the electron transport between the STM needle and the Si surface, both coated by water and hydrocarbon molecules adsorbed from the air. The basic method for monitoring the conduction mechanism in the STM needle–surface gap and inspecting the quality of surface cleaning from the adsorbed contaminates is to detect the STM current for various needle-surface distances [1, 2]. Stimulated adsorption can be prevented by carrying STM measurements in a pure neutral-gas environment.

Passivation of Si surface also results from high-dose iron-group ion implantation [5]. A thin metal-silicide layer thus produced protects Si from becoming oxidised, allowing high-quality STM images after years of keeping samples in air.

An ion- or laser-exposed surface generally develops a microstructure whose roughnesses may be of a comparable size to the needles. Since STM and AFM images are essentially convolutions of the images of the surface and the probing needle, this leads to considerable deviations of the experimental images from the real ones. In this connection, a problem arises as to how to estimate the STM and AFM image distortions due to the finite needle size. Computer imaging simulation has shown that knowing the real shape of the STM/AFM needle allows one to assess the reliability of images of surfaces with a developed microrelief [6].

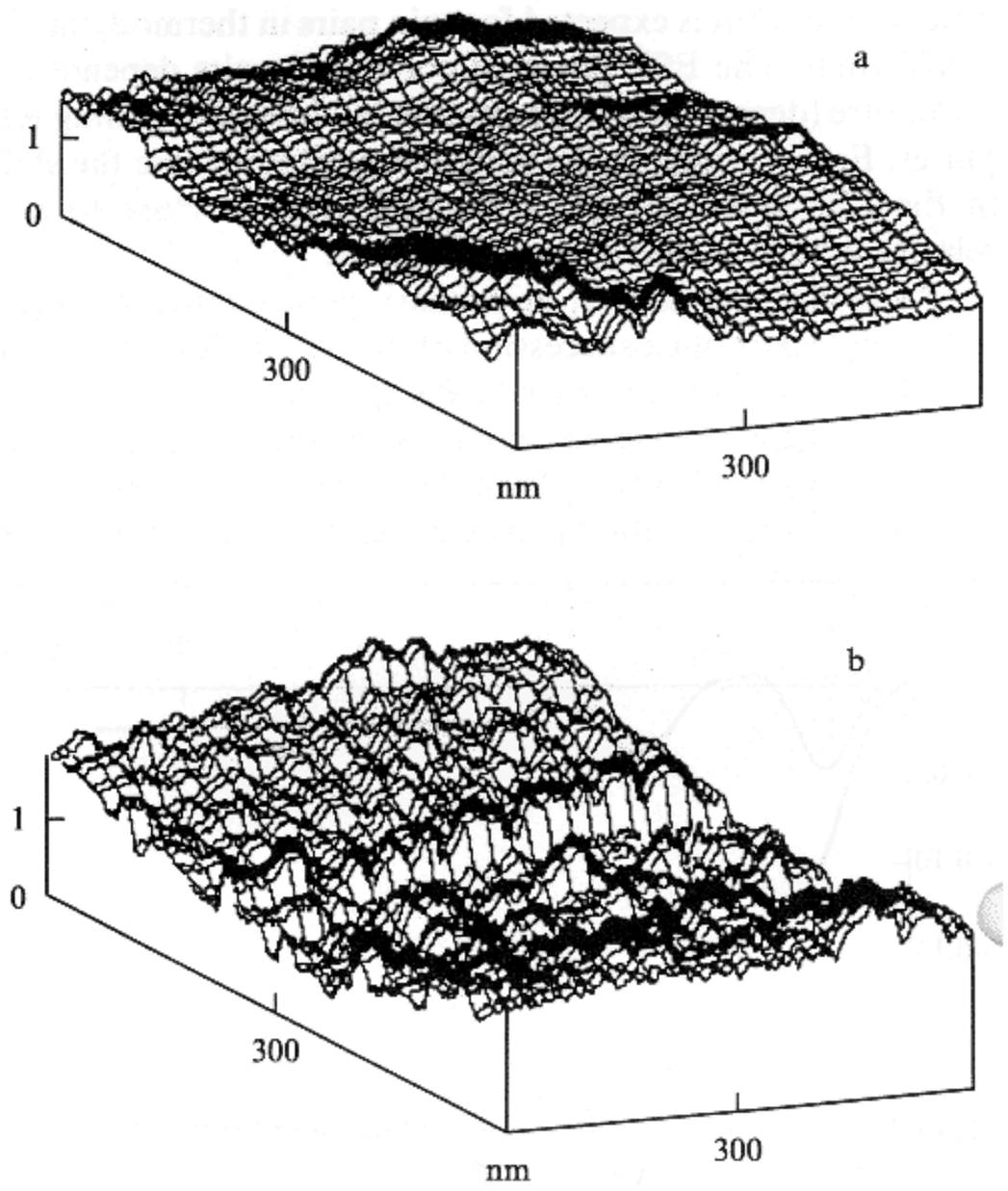

Figure 1. STM image of Si surface immediately after passivation (a), and after 40-min air exposure (b) in the electric field of the STM needle.

It would be most interesting, in our view, to try to deconvolve the obtained image, i.e., to solve the problem inverse to the convolution of the needle and surface images. Knowing the actual needle shape (from electronic microscopy, for example), the experimental image can be brought much closer to the real one. Conversely, using a sample with roughnesses of predetermined shape and size preliminarily produced on it, the image of the actual scanning STM needle can be reproduced. With the needle shape and size thus obtained, surfaces of unknown relief can be studied and, via the deconvolution procedure, AFM image distortions eliminated.

An original computer deconvolution method we proposed in Ref. [7] reduces significantly the needle-shape-related distortions and, for a prescribed microrelief, enables the image of the probe needle tip to be obtained. Fig. 2 illustrates the computer realisation of the method for a hemispheric surface protrusion imaged by a pyramidal AFM needle. It is clearly seen that after deconvolution the corrected AFM image (Fig. 2c) is much closer to the original one. Given the size of the hemisphere, in the same way the deconvolution of the images of the hemispheric protrusion and the AFM needle (Fig. 2b) yields the image of the AFM needle tip (Fig. 2d). If the scanning needle touches all points of the surface, the method eliminates all the distortions arising from the finite size and the shape of the needle [7].

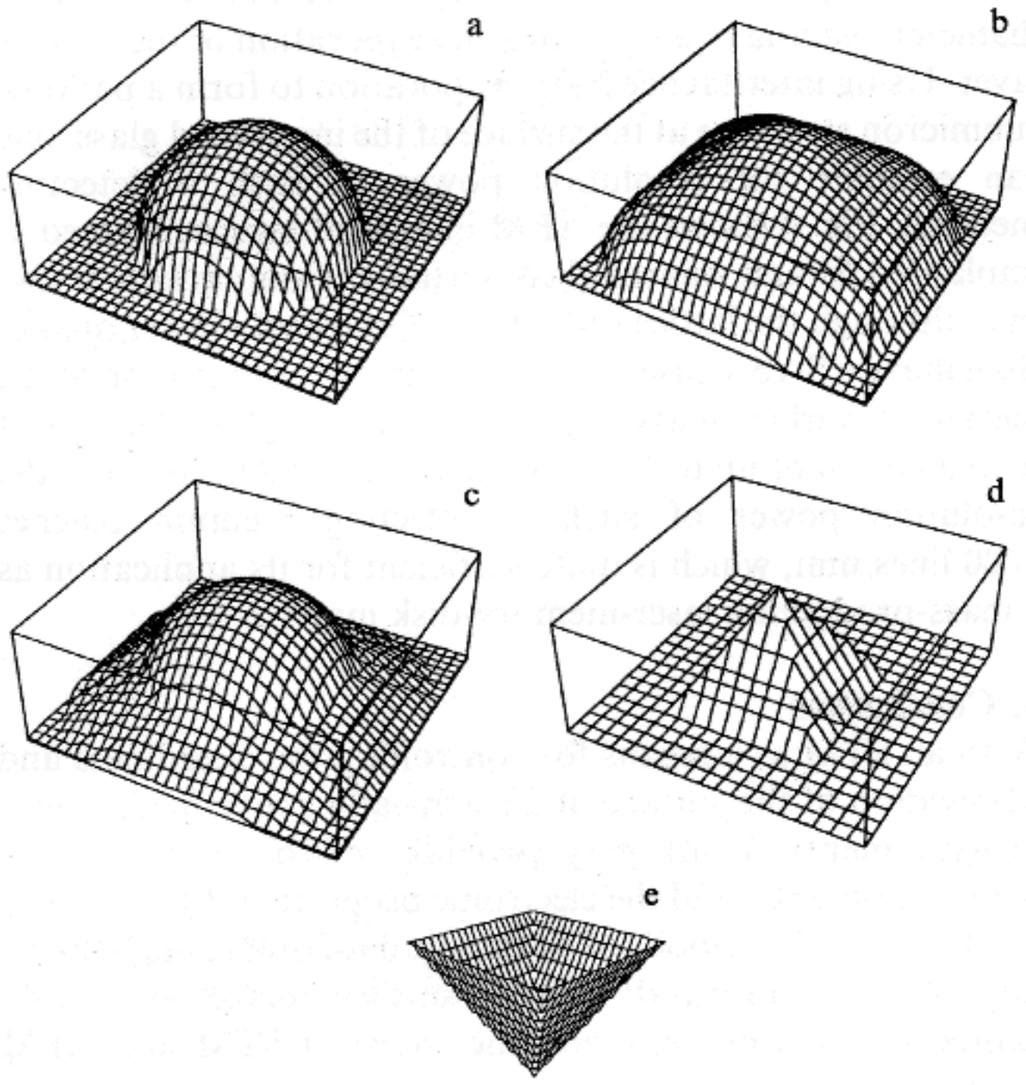

Figure 2. Computer correction for the distortion of the AFM image of a hemispheric protrusion, and AFM-needle shape determination via the deconvolution method: (a) initial surface, (b) its AFM image, (c) deconvolution-corrected AFM image, (d) AFM needle image obtained from (b) by the deconvolution method, (e) shape of the needle used in obtaining the AFM image (b).

The STM used was developed by the KFTI tunnelling microscopy group [8, 9]. Its distinguishing feature is that one and the same portion of the surface yields a dc-regime relief image and the distribution of electronic characteristics simultaneously. In the latter case, scanning each of the 128×64 surface points involves a 100-ms break of the STM feedback and a 50-ms measurement of the current-voltage characteristic (CVC), the latter reflecting the electronic properties of the Si area under the STM needle. To secure the required measuring rate, the CVCs are mapped via the integral parameter $Q = \int |I(V)| \, dV$. As shown in Refs [8, 9], an increase in Q corresponds to an increase in the conductivity in the semiconductor surface layer due to (i) recrystallisation of the amorphous silicon on heating and (ii) the electroactivation of the implanted impurity. The image characterising the surface distribution of conductivity is obtained in the same way as the ordinary dc-regime STM image, except that the quantity Z describing the relief height at a given point is replaced by the Q value at this point.

In both silicon and quartz-glass surface imaging, the Zelenograd 'Nanotekhnologiya — MDT' atomic-strength microscope P4-SPM was used.

Periodic structures were obtained [10] by two-beam holography with the use of a pulsed ruby laser. After a single 10-ns exposure to two (simultaneous) coherent laser beams, an interference light field formed at the sample surface. In the intensity-modulated field, spatially nonuniform surface heating with concomitant nonuniform melting, evaporation, or recrystallisation took place, with the result that the interference pattern persisted after the pulse, either as a periodic relief or a periodic variation of surface conductivity.

The samples used were Si (111) single-crystal plates KEF-4.5 implanted with 30-keV Sb^+ ions at doses above the amorphisation threshold, and polished plates of optical quartz glass implanted with Fe^+ ions (40 keV, 4×10^{17} ion$\times$ cm^{-2}). Prior to STM measurements, the Si samples were cleaned and passivated by hydrogenating in a dry nitrogen atmosphere as described in [1].

3. Microtopography and electronic properties of implanted semiconductors and glasses following pulsed interference laser exposure

When implanted Si or glass were subjected to a pulsed interference light field, one-dimensional, submicron periodic structures (lattices) generally formed on their surfaces, whose period was described fairly well by the familiar expression $d = \lambda / [2 \sin(\alpha/2)]$, where λ is the laser wavelength, and α, the angle between the beams incident onto the surface [9].

Comparison of silicon STM and STS images showed that, for energy densities above 1 J cm^{-2}, STM lattice images with a relief height of about 40 nm were seen, although no marked changes in the parameter Q were observed in this portion of the surface. In this case the large-depth evaporation of Si and the complete recrystallisation of the whole of the surface apparently combine to form a microrelief with practically constant conductivity along the surface. At a density of about 1 J cm^{-2}, simultaneous STM and Q periodic structure images were usually observed, STM protrusions corresponding to high-conductivity surface portions. Finally, for incident radiation densities below 1 J cm^{-2}, virtually no STM lattices were visible, whereas in the Q image a distinct 0.9-μm-periodic structure appeared [10]. In the latter case we believe that rather than Si evaporation, local recrystallisation of the amorphous surface layer of Si at light field energy antinodes occurs ('interference laser annealing'). Since the density of the implantation-amorphised Si is only by 2 – 3% lower than for crystalline Si, the recrystallisation of the 20-nm amorphous layer should not produce a noticeable microrelief.

In the central portion of some of the holographic Si-surface lattices, two-dimensional periodic structures were detected by both AFM and STM techniques [10]. In the

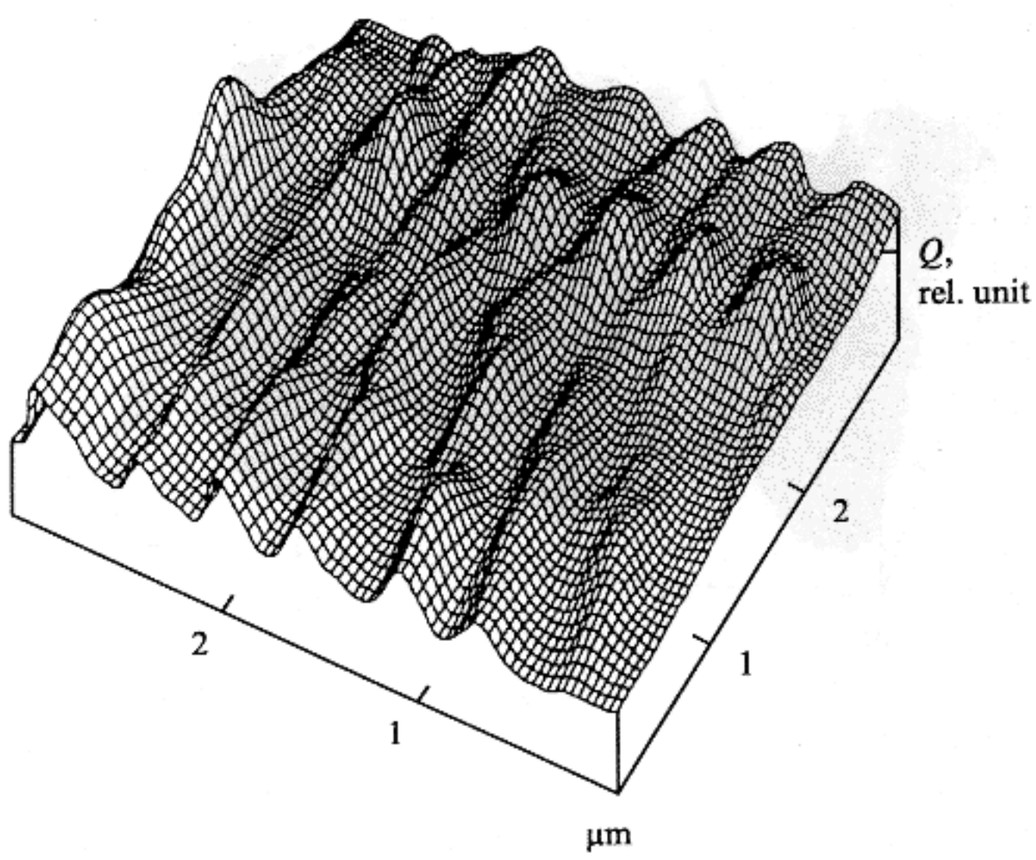

Figure 3. STS image (in terms of the parameter Q) of the surface conductivity of implanted Si after a pulsed interference laser annealing.

STM measurements they were most clearly discernible as a change in the parameter Q (Fig. 3), the period of such lattices being half that in their one-dimensional counterparts. Such two-dimensional structures have been known for quite a long time [11] and are believed to arise from the interference between the incident electromagnetic wave and the electromagnetic surface wave it generally excites in a metal (semiconductors are assumed to become metallic when melted by a laser beam). There exist, however, alternative models for the formation of such two-dimensional structures by a laser beam [11].

Local changes in the absorption and reflection coefficients during fixed depth evaporation provide the basis for binary information recording with a 0.8 – 1-μm-focused laser beam when manufacturing the optical memory disks. Due to its high mechanical and chemical resistance, the implantation-produced granular metallic film buried in the surface glass layer is very promising for the purpose [4]. The resolution power of such a detecting medium is as yet, however, unclear, because the randomly distributed optical absorption centres (metallic Fe particles) may be as large as tens of nanometers in diameter, leading to a nonuniform evaporation of the surface layer. Using interference laser evaporation to form a periodic submicron structure at the surface of the implanted glass, one can estimate the resolution power of such a detecting medium. Fig. 4 shows the AFM images of lattices formed at implanted Si and quartz-glass surfaces. Comparison shows that although the lattice on glass is of markedly lower quality than that on Si (because of the nonuniform evaporation of the metal-rich surface glass layer), still even on glass the lattices with a period of up to 1 μm are possible. This means that the resolution power of such a detecting medium reaches 1000 lines/mm, which is quite sufficient for its application as a mass-production laser-memory-disk matrix.

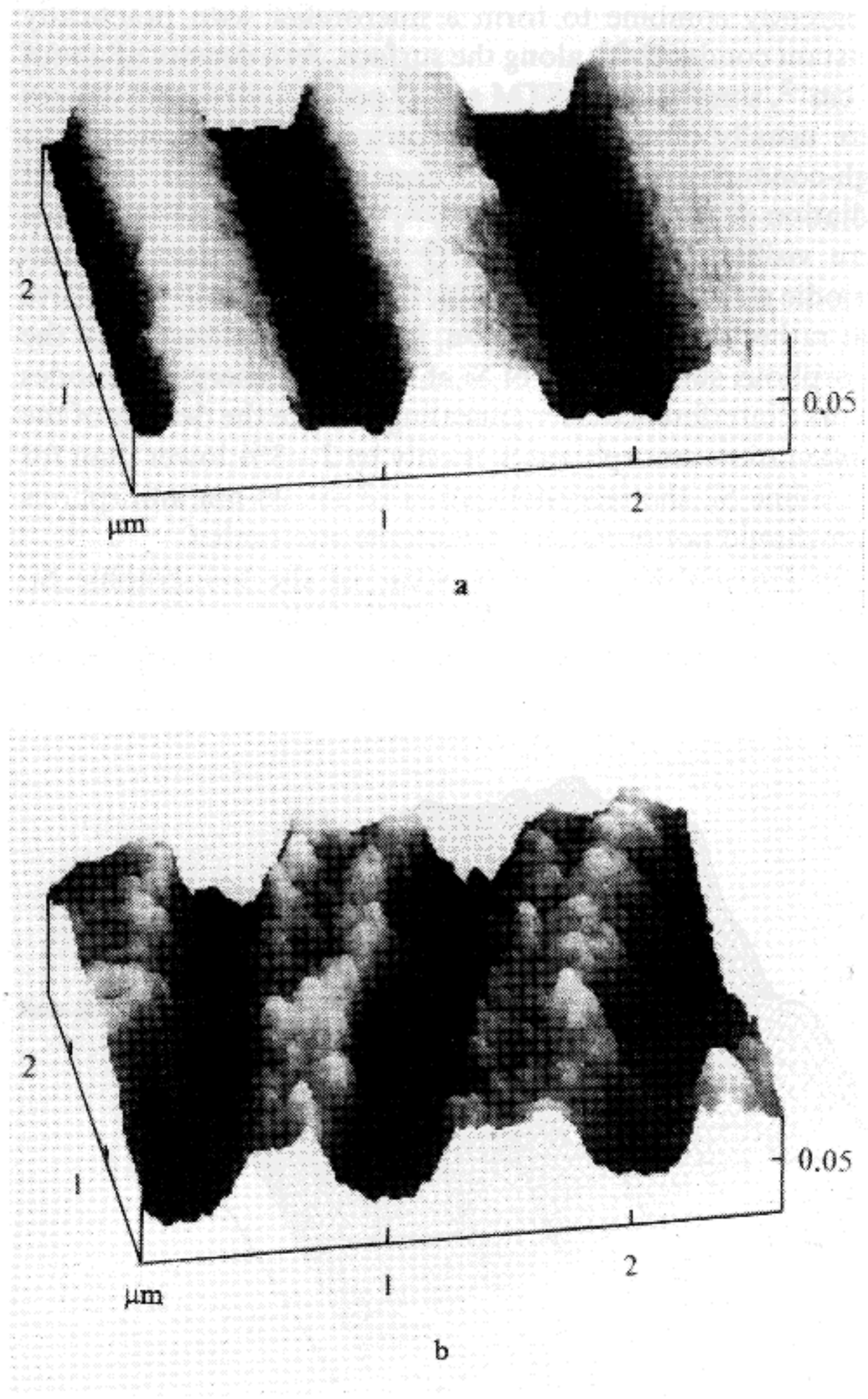

Figure 4. AFM image of one-dimensional periodic structures at the surface of implanted Si (a) and glass (b) formed by pulsed-interference laser evaporation.

4. Conclusions

With an STM as a means for controlling the cleanliness and passivation of the surface of a chemically active media, even measurements in air may provide reliable data on the microtopography and the electronic properties of the surface.

The current methods of electronic data processing make it possible to significantly reduce surface image distortions caused by the finite size and the shape of STM and AFM needles.

The high spatial resolution of STMs and AFMs makes it possible to study fine details of the light-surface interaction, in particular to investigate how the size of optical absorption centres affects the formation of a submicron periodic relief on the surface during its laser-stimulated local evaporation.

Finally, STS measurements allow a visualisation of one- and two-dimensional periodic conductivity variations produced by pulsed-interference laser annealing in a surface layer of Si.

The work has been supported in part by the Ministry of Science and Technological Policy of the Russian Federation (project No 143/57/4), and by the Academy of Sciences of Tatarstan (project No 04-12/95).

References

1. Bukharaev A A et al. *Poverkhnost'* **12** 69 (1994)
2. Bukharaev A A et al. *J. Vac. Sci. Technol. B* **13** 1274 (1995)
3. Bukharaev A A et al. *Fiz. Tverd. Tela* **33** 1018 (1991) [*Sov. Phys. Solid State*]
4. Certificate of Authorship 1231818 USSR *Patentnyi Bull.: Izobreteniya* **18** 256 (1995)
5. Bukharaev A A et al. *Pis'ma Zh. Tekh. Fiz.* **16** 8 (1990) [*JTP Letters*]
6. Bukharaev A A *Zavodskaya Laboratoriya* **10** 15 (1994)
7. Certificate of Authorship 4916118 USSR *Patentnyĭ Bull.: Izobreteniya* **44** 171 (1992)
8. Bukharaev A A et al. *Phys. Status Solidi A* **131** 79 (1992)
9. Bukharaev A A et al. *Poverkhnost'* **4** 104 (1993)
10. Bukharaev A A et al. *Opt. Spektrosk.* **79** 417 (1995) [*Opt. Spectrosc.* (Russia)]
11. Akhmanov S A et al. *Usp. Fiz. Nauk* **147** 675 (1985) [*Sov. Phys. Usp.* **28** (12) 1084 (1985)]